

UniDCP: Unifying Multiple Medical Vision-language Tasks via Dynamic Cross-modal Learnable Prompts

Chenlu Zhan, Yufei Zhang, Yu Lin, Gaoang Wang *Member, IEEE*, Hongwei Wang *Senior Member, IEEE*

Abstract—Medical vision-language pre-training (Med-VLP) models have recently accelerated the fast-growing medical diagnostics application. However, most Med-VLP models learn task-specific representations independently from scratch, thereby leading to great inflexibility when they work across multiple fine-tuning tasks. In this work, we propose UniDCP, a Unified medical vision-language model with Dynamic Cross-modal learnable Prompts, which can be plastically applied to multiple medical vision-language tasks. Specifically, we explicitly construct a unified framework to harmonize diverse inputs from multiple pre-training tasks by leveraging cross-modal prompts for unification, which accordingly can accommodate heterogeneous medical fine-tuning tasks. Furthermore, we conceive a dynamic cross-modal prompt optimizing strategy that optimizes the prompts within the shareable space for implicitly processing the shareable clinic knowledge. UniDCP is the first Med-VLP model capable of performing all 8 medical uni-modal and cross-modal tasks over 14 corresponding datasets, consistently yielding superior results over diverse state-of-the-art methods.

Index Terms—Medical Vision-language Pre-training, Dynamic Cross-modal Prompts, Cross-modal Shareable Space

I. INTRODUCTION

MEDICAL image analysis with deep learning has significantly enhanced its application in medical practice. However, these medical multi-modal models for medical diagnostic analysis require extensive training on a multitude of diverse medical datasets. This entails time-consuming and complex manual annotation costs, posing a significant impediment to the development of intelligent medical diagnostics. Recently, advances in medical vision-language pre-training models (Med-VLP) [1]–[6] have significantly improved the efficiency of the medical diagnostics tasks. The Med-VLP model aims to learn unified representations from large-scale medical clinic image-text pairs. These representations with task-specific parameters are then fine-tuned for the medical downstream tasks (e.g. medical question answering task, medical report generation task).

However, most recent Med-VLP works [1], [2], [5]–[8] learn proprietary representations corresponding to fine-tuning

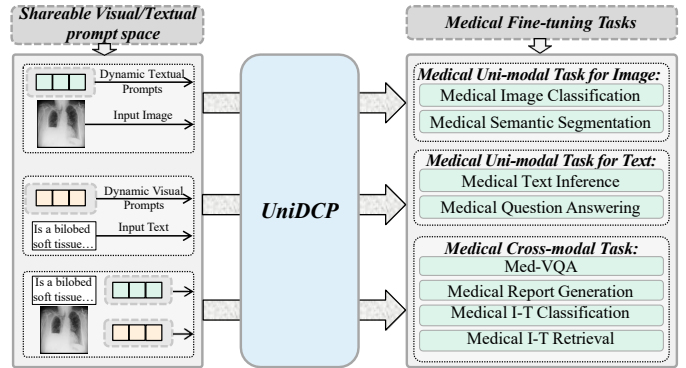


Fig. 1. UniDCP is a unified and plastic model capable of multiple medical uni-modal and cross-modal tasks with dynamic shareable cross-modal prompts. The broad unification is achieved by harmonizing diverse inputs of heterogeneous tasks with the dynamic visual and textual prompts which are selected from the corresponding shareable space.

tasks, which results in the inflexibility of Med-VLP model across multiple fine-tuning tasks due to task-specific structures or static components. Equipped with task-specific structures, some works [9]–[11] grasp fine-grained representations within two-stream branches for medical classification tasks, and the others [7], [12] introduce exclusively aligned frameworks for the medical cross-modal reasoning tasks. This trend constrains the transferability of the Med-VLP model with limited concept knowledge. Besides, some works [13]–[15] introduce the visual and textual prompts into vision-language tasks, which transfer the well-optimized models to fine-tuning tasks. Although these works express superior generalization ability in downstream tasks, the learned prompts remain static, exclusively benefit the individual fine-tuning task and reflect restrictions for the others. It remains an open problem to construct a unified and plastic Med-VLP model that can simultaneously adapt to multiple medical tasks.

To address the challenges above, we propose **UniDCP**, a **Unified Med-VLP** model via **Dynamic Cross-modal learnable Prompts**, which is capable of simultaneously performing diverse medical uni-modal and cross-modal fine-tuning tasks. Specifically, we construct a unified model within a triple-stage prompt scheme: the cross-modal prompt initialization, multi-task pre-training and multi-task adaptation. As shown in Fig. 1, the unified model is scaled by harmonizing diverse inputs from multiple pre-training tasks via the initialized cross-modal prompts, which consequently enables the handling of diverse medical fine-tuning tasks with no task-specific param-

This work was supported in part by Zhejiang Provincial Natural Science Foundation of China (LDT23F02023F02).

Chenlu Zhan is with the College of Computer Science and Technology, Zhejiang University, Zhejiang, China (chenlu.22@intl.zju.edu.cn)

Yufei Zhang is with College of Biomedical Engineering and Instrument Science, Zhejiang University, Zhejiang, China (yufei1.23@intl.zju.edu.cn)

Yu Lin, Gaoang Wang and Hongwei Wang are with Zhejiang University-University of Illinois Urbana-Champaign Institute, Zhejiang University, Haining, China. (yulin@intl.zju.edu.cn, gaoangwang@intl.zju.edu.cn, hongwei-wang@zju.edu.cn)

eters. Furthermore, we initiatively present the dynamic visual-textual prompts optimizing strategy for resiliently cooperating multiple tasks with the shareable clinic knowledge. In contrast to static prompts, we encode visual/textual prompts into a key-value shareable space, where dynamic optimization occurs by selecting a subset of the most relevant prompts through the query function. The key-value setting is devised for dynamic prompts strategy which links the prompts as key-value pairs and adopts the query function for semantic prompts selection. It is superior in medical cross-modal knowledge extraction and alignment. Then we adapt the unified model and the dynamic prompts with shareable clinic knowledge into multiple medical fine-tuning tasks. During these processes, the clinic knowledge is acquired from two aspects: 1) The dynamic prompts with the most pertinent medical information are retrieved through a query function. 2) The selected prompts consecrate with visual/textual representations that plastically adapt shareable clinic knowledge into multiple tasks. We conduct comprehensive experiments on medical vision-language understanding benchmarks which conclude 8 uni-modal/cross-modal fine-tuning tasks and 14 corresponding medical datasets. Extensive experiments demonstrate the superiority of the proposed model in plastically integrating clinic-shareable knowledge into diverse medical vision-language tasks within a unified structure. Overall, the proposed UniDCP is a integrated and flexible model with low-cost expansion. 1) Integration: UniDCP has wider generalization in various-modality tasks with no task-specific modules and achieves all-sided SOTA results. 2) Flexibility: We propose dynamic prompts to select the most semantically effective representations for each task, which scalably adapts to various tasks with negligible overhead. Our contributions are summarized as follows:

- We propose UniDCP, a unified and plastic model capable of multiple medical fine-tuning tasks by harmonizing heterogeneous inputs from multiple pre-training tasks via cross-modal prompts.
- We present the dynamic cross-modal prompts optimizing strategy within shareable space to cooperate with shareable clinic knowledge under different task transitions.
- UniDCP is the first Med-VLP model that attains state-of-the-art results on 8 medical vision-language tasks with 14 benchmarks, illustrating the superiority in integrating the shareable clinic knowledge into multiple tasks.

II. RELATED WORKS

A. Medical Vision-language Pre-training

Medical vision-language pre-training (Med-VLP) aims to learn the cross-modal representations from large-scale medical image-text pairs. Current Med-VLP methods [1], [4]–[7], [9], [16], [17] employ task-specific pre-training strategies to learn proprietary representations, such as the fine-grained representations for classification and the aligned cross-modal representations for reasoning. For the former strategy, GLoRIA [9] presents an efficient medical image recognition method by evaluating the local similarity between image sub-regions and words. REFERS [10] enhances medical visual information by adopting multiple visual views. MedKLIP [11]

introduces a triplet extraction module designed to retrieve medical-related details from reports for reinforcing the classification ability. For the latter, MRM [12] acquires the aligned visual knowledge-enhanced representations with the direct incorporation of cross-modal visual information processed by GAP into report reconstruction. M3AE [7] devises various aligned supervised pre-training tasks for obtaining medical cross-modal domain expertise, which is a very similar setting to ours. These works all focus on learning superior specific representations tailored to corresponding downstream tasks but pose a challenge in consolidating the Med-VLP model for multiple fine-tuning tasks and inhibiting its universal applicability. There remains a gap in constructing a Med-VLP framework that has superior plasticity and transferability to multiple medical vision-language tasks within a unified model.

B. Prompt Tuning

The prompt tuning [18]–[20] is initially introduced by the NLP community to promote the efficiency of the large pre-trained model on fine-tuning language tasks. Recent works [13], [16], [21], [22] also explore the prompt tuning in vision-language tasks. CoOp [13] designs the learnable prompts with context words and achieves obvious improvements with few labeled images. VPT [21] turns patches of images into learnable prompts to efficiently fine-tune the large-scale transformer models in vision tasks. UPT [15] introduces two sets of vision-language prompts for fine-tuning the vision-language models. CLIP-Adapter [16] introduces an adapter module to embed the text and image features into the same space for better adaptation of various datasets. Although these static prompt tuning works have superior efficiency in fine-tuning tasks, they restrictively remain static when applied to exclusive downstream tasks independently. It motivates us to explore learnable dynamic cross-modal prompts which can be adapted to various medical fine-tuning tasks with shareable clinic knowledge. There are two key innovations that distinguish our work from others [13], [15], [21], [23]: 1) UniDCP is a comprehensive yet low-cost model that seamlessly handles various medical multi-modal and single-modal tasks with dynamic visual/textual prompts while other models with expensive-cost lack the processability of text-only tasks. 2) Besides the multi-modal prediction, classification, segmentation, etc, UniDCP ventures into medical generation task and exhibits better performance.

III. METHODOLOGY

In this section, we propose UniDCP, which is a unified and plastic model for multiple medical vision-language tasks. Fig. 2 illustrates the overview of triple-stage procedures which contains the visual-textual prompt initialization, multi-task pre-training and multi-task adaptation.

A. Problem Setup

Med-VLP aims to learn medical vision-language representations from clinic images and paired radiology reports. Some works introduce prompts P that can transfer well-optimized models to fine-tuning tasks. Within the pre-training

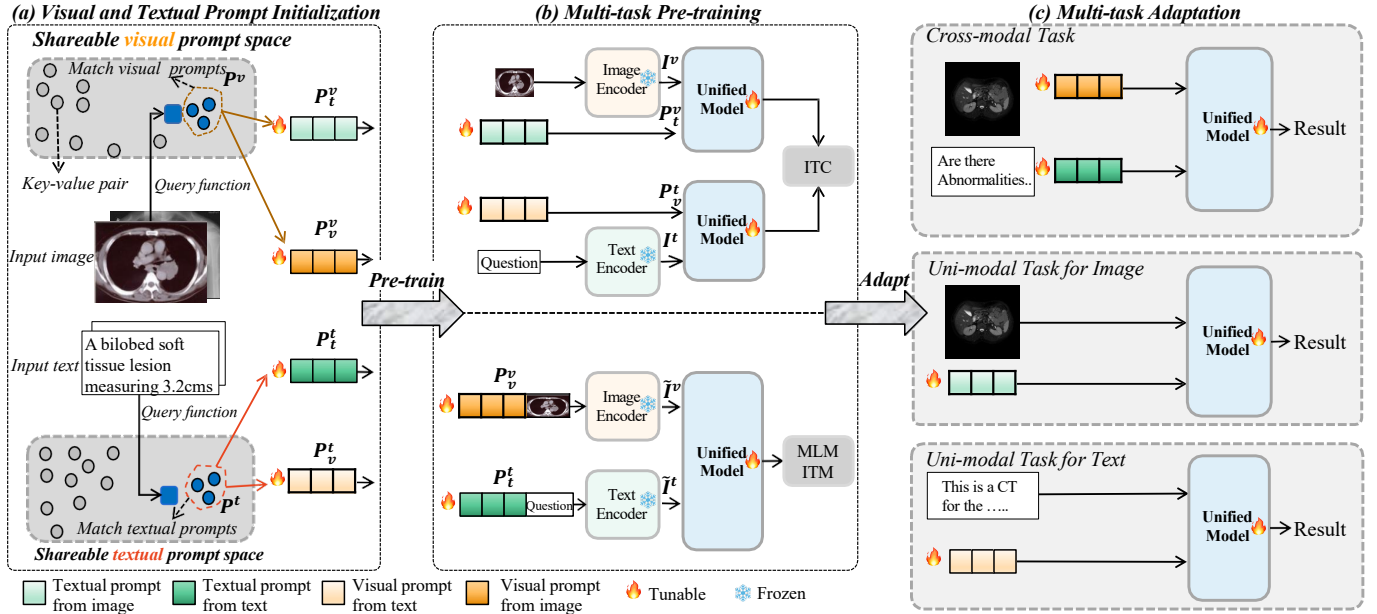


Fig. 2. The network structure of UniDCP. (a) Within a unified model, the visual and textual prompts are introduced from the shareable visual prompt space to unify the inputs. The cross-modal prompts are initialized by drawing the chosen feature nearer to the respective prompts through the query function. (b) After unifying the inputs with the visual/textual prompts, the unified model is optimized with the cross-modal and uni-modal pre-training tasks. (c) The unified model, which incorporates the dynamic visual and textual prompts is adapted to the cross-modal tasks and the uni-modal tasks for text and image.

model U , the medical inputs I may consist of the text-only embedding input $I^t \in \mathbb{R}^{D_t \times L_t}$, image-only embedding input $I^v \in \mathbb{R}^{D_v \times L_v}$ and image-text pairs, where L_t , L_v and D_t , D_v are the token lengths and the embedding dimension of the textual and visual features. The representations are learned with the pre-trained model from R pre-training tasks, which can be formulated as:

$$\hat{\mu}, \hat{\mu}_1, \dots, \hat{\mu}_R, \hat{\theta} = \arg \max_{\mu, \mu_1, \dots, \mu_R, \theta} \sum_{r=1}^R \mathcal{L}_r(Y_r, \mathcal{H}_{\mu_r}(U_\mu(I, P_\theta))) \quad (1)$$

where \mathcal{H}_{μ_r} represents the prediction heads with corresponding trainable parameters μ_r , Y_r is the ground-truth labels and \mathcal{L}_r is the loss function of the pre-training tasks r . U_μ is the pre-trained model which is parameterized by μ . P_θ represents the prompts with tunable parameter θ .

For constructing a unified model U_μ that can apply to multiple medical fine-tuning tasks, the issue lies in enabling the unified model to effectively handle variable inputs and grasp the shareable knowledge.

B. Visual and Textual Prompts Initialization

To promote compatibility of the model, we unify the inputs I by introducing the visual prompt P^v for the text-only embedding input I^t and the textual prompt P^t for the image-only embedding input I^v , respectively.

$$I = \begin{cases} (I^v, P^t) & \text{if image-only} \\ (P^v, I^t) & \text{if text-only} \\ (I^v, I^t) & \text{if image-text} \end{cases} \quad (2)$$

where $P^t \in \mathbb{R}^{D_t \times N}$, $P^v \in \mathbb{R}^{D_v \times N}$ and N represents the number of the learnable prompts.

Moreover, in contrast to static prompts tailored for each independent medical downstream task, we introduce dynamic

cross-modal prompts that plastically incorporate shareable clinic visual/textual knowledge into multiple medical downstream tasks. Formally, we first construct the shareable visual and textual prompt space P^v , P^t to store the transferable clinic prompt knowledge. The proposed shareable prompt space exactly serves as a cross-modal representation repository that adapts the most effective representations for various fine-tuning tasks through the dynamic strategy, which can be defined as:

$$\begin{aligned} P^v &= \{p_1^v, p_2^v, \dots, p_M^v\} \\ P^t &= \{p_1^t, p_2^t, \dots, p_J^t\} \end{aligned} \quad (3)$$

where M , J is the total number of the visual and textual prompts in each space respectively, $p_i^v \in \mathbb{R}^{D_v \times L_v^p}$, $p_j^t \in \mathbb{R}^{D_t \times L_t^p}$ are the single visual and textual prompt with the token length L_v^p , L_t^p , and embedding sizes D_v , D_t are same as the corresponding inputs.

Following the VQ-VAE [24], we further devise the cross-modal prompts query strategy for selecting the most effective N prompts from the corresponding shareable prompt space, applying to unify the inputs. Specifically, we link each visual/textual prompt as the trainable key-value pair: $\{(k_1^v, p_1^v), \dots, (k_M^v, p_M^v)\}$ and $\{(k_1^t, p_1^t), \dots, (k_J^t, p_J^t)\}$, where the $k_i^t \in \mathbb{R}^{D_t}$ and the $k_j^v \in \mathbb{R}^{D_v}$. Thus we adopt the query function q to encode the visual/textual feature into the same dimension \mathbb{R}^{D_t} and \mathbb{R}^{D_v} as the key in the key-value pair. With the visual and textual embedding inputs I^v and I^t , we query the top- N keys with the query function q :

$$\begin{aligned} P^t &= \arg \max_{\{s_i\}_{i=1}^N \subseteq [1, M]} \sum_{i=1}^N \gamma(q(I^t), k_{s_i}^t) \\ P^v &= \arg \max_{\{s_i\}_{i=1}^N \subseteq [1, J]} \sum_{i=1}^N \gamma(q(I^v), k_{s_i}^v) \end{aligned} \quad (4)$$

where the $\{s_i\}_{i=1}^N$ is the subset of length N , the γ represents the matching function that computes the cosine similarity between the key-value prompt and the query to select effective prompts. Overall, the surrogate loss L_p for drawing the chosen keys nearer to their respective query features can be denoted:

$$L_p = \sum_{P^t} \gamma(q(I^t), k_{s_i}^t) + \sum_{P^v} \gamma(q(I^v), k_{s_i}^v) \quad (5)$$

C. Multi-task Pre-training

To accommodate diverse pre-training tasks with various inputs, we treat the visual prompt P^v as P_t^v and P_v^v , the textual prompt P^t as P_t^t and P_v^t , playing distinct roles related to vision and text when the text-only and image-only input, respectively. We can both unify various inputs and adapt cross-modal inputs into \tilde{I}^v and \tilde{I}^t by concatenating the inputs and the prompts P_v^v , P_t^t along D_v and D_t dimension respectively. This allows us to optimize the same unified model with multiple pre-training tasks, as illustrated in Fig. 2 (b). Following the VisualBert [25], we employ the masked language modeling (MLM), image-text matching (ITM) and image-text contrast (ITC) tasks for optimizing the unified model U . For MLM and ITM, dynamic prompts are also concatenated with image/text embeddings to facilitate cross-modal alignments.

1) *MLM*: The MLM pre-train task randomly masks 15% input words Y_{MLM} and the optimization object across the inputs \tilde{I}^v and \tilde{I}^t is:

$$L_{MLM} = - \sum_{(\tilde{I}^v, \tilde{I}^t)} \log f_s(H_{MLM})(Y_{MLM}|\tilde{I}^v, \tilde{I}_M^t) \quad (6)$$

where H_{MLM} represents prediction heads of MLM, f_s is the softmax layer, \tilde{I}_M^t is the remaining text input.

2) *ITM*: The ITM task randomly selects positive and negative image-text pairs into the encoder, proposing to figure out the matching degree of the input image and text features. The final probability p_{ITM} can be calculated by the output of the softmax layer with the concatenation of the representations of the image-text pairs $z_{[CLS]}^v$ and $z_{[CLS]}^t$. The optimization objective of ITM is defined as:

$$L_{ITM} = - \sum_{(\tilde{I}^v, \tilde{I}^t)} \log p_{ITM}(Y_{ITM}|\tilde{I}^v, \tilde{I}^t) \quad (7)$$

3) *ITC*: The ITC task adopts the dual-encoder to explore the best cross-modal representation through computing the similarity between image-to-text p_n^{i2t} and text-to-image p_n^{t2i} . The optimization objective of ITC is defined as:

$$L_{ITC} = -\frac{1}{2} \sum_{(I^v, P_t^v)} \log p^{i2t}(Y^{i2t}|I^v, P_t^v) - \frac{1}{2} \sum_{(I^t, P_v^t)} \log p^{t2i}(Y^{t2i}|I^t, P_v^t) \quad (8)$$

where Y^{i2t} , Y^{t2i} are ground-truth labels which set to 0 for the negative pair and 1 for the positive pair. Overall, the total optimization L_{pre} of the multi-task pre-training consists of three loss terms:

$$L_{pre} = L_{MLM} + \sigma L_{ITM} + \lambda L_{ITC} + \beta L_p \quad (9)$$

where σ , λ , β are hyperparameters for balancing the loss terms.

D. Multi-task Adaptation

As shown in Fig.2 (c), leveraging a unified model that incorporates the dynamic visual and textual prompts, we apply it to cross-modal and uni-modal medical vision-language fine-tuning benchmarks. For the report generation, our unified model extracts image representations and then combines them with text prompts. The concatenations are fed into a transformer decoder (except cross-attention layers) initialized from a pre-trained language encoder.

Specifically, initialized from the pre-trained model U , we utilize the combined representations of image/visual prompt \tilde{I}^v and text/textual prompt \tilde{I}^t as input for prediction in the medical cross-modal task. For the medical uni-modal task for image/text, we unify the input with the contrary dynamic prompt and then feed the sequence $(I^v, P_t^v)/(P_v^t, I^t)$ to the unified model with initialized parameters.

IV. DATASETS AND IMPLEMENTATION DETAILS

A. Pre-train Datasets and Configurations

We pre-train the proposed framework with the ROCO [26] and MIMIC-CXR [27] datasets. The ROCO [26] is the large-scale public medical image-text dataset that includes 81,000 radiology images of various modalities. The MIMIC-CXR [27] is a large X-ray dataset that concludes 377,100 radiology images of the chest and 227,835 corresponding reports from patients. We all follow the official splitting.

B. Medical Fine-tuning Datasets

We conduct medical vision-language benchmarks which conclude 8 medical cross-modal and uni-modal tasks with 14 fine-tuning medical datasets.

1) *Medical Vision Question Answering*: VQA-RAD [28] comprises 315 radiology images sourced from PubMed, alongside 3,515 question-and-answer pairs meticulously curated by clinicians. We follow the original splitting which contains 3064 training samples and 451 samples for testing. SLAKE [29] concludes 642 radiology images and 7,033 question-and-answer samples across 39 organs. We adopt the official splitting of 70% training pairs and 30% testing pairs. Path-VQA [30] is a pathology dataset for Med-VQA which contains 4,998 pathology images with 32,795 question-answer pairs. The image-question pairs are composed of 8 types of questions.

2) *Medical Report Generation*: IU X-Ray [31] is the predominant dataset employed for the medical report generation task, which contains 7,470 chest X-ray images and 3,955 related clinic reports. The MIMIC-CXR [27] dataset encompasses 377,100 radiology images of the chest, along with 227,835 corresponding reports from patients. We use the train-set of MIMIC-CRX for fine-tuning and the test-set for evaluation.

3) *Medical Image-Text Classification*: MELINDA [32] is a multi-modal biomedical dataset that includes 2833 medical images paired with corresponding captions. We follow the official data splitting with 80%-10%-10% of train-set, validation-set and test-set respectively.

TABLE I

THE COMPARISONS BETWEEN UNIDCP AND SOTA MED-VQA METHODS. "OPEN": OPEN-ENDED QUESTIONS WITH NO FIXED FORM ANSWER. "CLOSED": CLOSED-ENDED QUESTIONS WITH A YES/NO ANSWER. -PMC-VQA: PRE-TRAIN ON THE PMC-VQA DATASET.

Methods	VQA-RAD(%)			SLAKE(%)			Path-VQA(%)		
	Open	Closed	All	Open	Closed	All	Open	Closed	All
MFB [33]	14.5	74.3	50.6	72.2	75.0	73.3	-	-	-
SAN [34]	31.3	69.5	54.3	74.0	79.1	76.0	1.6	59.4	30.5
BAN [35]	37.4	72.1	58.3	74.6	79.1	76.3	2.9	68.2	35.2
MAML+SAN [36]	38.2	69.7	57.1	-	-	-	5.4	75.3	40.5
MAML+BAN [36]	40.1	72.4	60.7	-	-	-	5.9	79.5	42.9
MEVF+SAN [37]	49.2	73.9	64.1	75.3	78.4	76.5	6.0	81.0	43.6
MEVF+BAN [37]	49.2	77.2	66.1	77.8	79.8	78.6	8.1	81.4	44.8
VQAMIX [3]	56.6	79.6	70.4	-	-	-	12.1	84.4	48.4
MMBERT [1]	58.3	76.9	66.9	-	-	-	-	-	-
CPRD+BAN [4]	52.5	77.9	67.8	79.5	83.4	81.1	-	-	-
MedVInT [38]	55.3	80.5	70.5	79.7	85.1	81.8	-	-	-
PubMedCLIP [2]	58.0	79.6	71.1	78.2	82.6	80.1	13.4	83.6	48.5
M3AE [7]	67.2	83.5	77.0	80.3	87.8	83.2	14.2	84.0	48.8
Ours	68.5\pm1.2	84.4\pm1.0	79.2\pm1.1	82.4\pm1.4	88.9\pm1.2	85.9\pm1.3	15.9\pm1.4	85.4\pm1.3	50.7\pm1.4
MedVInT-PMC-VQA [38]	73.7	86.8	81.6	84.5	86.3	85.2	-	-	-
Ours-PMC-VQA	74.5\pm1.1	87.9\pm1.0	82.7\pm1.1	85.8\pm1.1	88.6\pm1.4	86.7\pm1.2	16.9\pm1.2	86.2\pm1.4	51.9\pm1.3

4) *Medical Image-Text Retrieval*: We filter the non-radiology samples of ROCO [26] and split the 65,460 medical image-caption pairs as the train-set, 8,183 and 8,182 samples as the validation-set and test-set respectively.

5) *Medical Image Classification*: CheXpert [39] is a large radiograph dataset with 224,316 radiographs. Since the private access of the test-set, following ConVIRT [40], we adopt the randomly selected 5000 radiographs of the train-set as the validation-set and take the validation-set as the test-set. RSNA Pneumonia [41] collects nearly 30,000 frontal chest X-rays. We split the dataset into 25184, 1500 and 3,000 of train-set, validation-set and test-set respectively.

6) *Medical Semantic Segmentation*: The SIIM Pneumothorax dataset [42] encompasses 12,047 chest radiographs. The dataset is partitioned into training, validation, and testing subsets, accounting for 70%, 30%, and 30% respectively. The RSNA [43] dataset follows the same split protocol. We transform the ground truth of object detection into masks suitable for semantic segmentation tasks.

7) *Medical Natural Language Inference*: MedNLI [44] is adopted for the clinic natural language inference task. We follow the original splitting which contains 11,232 training samples, 1,395 development samples, and 1,422 test samples.

8) *Medical Question Answering*: PubMedQA [45] is a biomedical question answering dataset selected from PubMed abstracts. PubMedQA consists of 1,000 instances expertly labeled, along with 61,200 unlabeled and 211,300 question-answer instances artificially generated. We select 450, 50, 500 question-answer instances for the train-set, validation-set, and test-set respectively. BioAsq [46]. The BioAsq is a biomedical dataset for the medical question answering task, which contains 618 training samples and 161 testing samples.

C. Implementation Details

UniDCP is trained with 6 NVIDIA 3090 GPUs. For pre-training, we adopt 12-layer transformer initialized from CLIP-ViT [47] and RoBERTa [48] as the vision and text encoder. The 6-layer transformer with 768 dimensions of hidden states and 12 heads is settled as the unified model. The model pre-trains 100,000 steps with AdamW optimizer whose learning

rate of vision and text encoder are $1e^{-5}$ and $5e^{-5}$ respectively, and the weight decay is $5e^{-4}$. We conduct the effect results of transformer layers in Fig. 6. The input images are cropped to 224×224 . The hyperparameters λ , β and σ of pre-training loss are set to 0.8, 0.9 and 0.9 respectively, the sensitivity results are in Fig. 6 and 5. The dimensions D_v and D_t of visual and textual embedding are 1024 and 768 respectively. The top-N in Eqn. 4 is set to top-5. The final M , J are all set to 1024. The total number N of learnable visual/textual prompts are set to 49 and 32 respectively.

Except for the accuracy of Med-VQA and medical text tasks, we adopt the commonly used NLG metrics for medical report generation, Dice score for medical semantic segmentation and AUC score for medical image classification.

V. EXPERIMENTS AND RESULTS

A. Comparison with State-of-the-art Methods

To demonstrate the effectiveness of UniDCP, we conduct abundant experiments on 8 medical cross-modal and unimodal tasks over 14 datasets in total.

1) *Medical Visual Question Answering*: We take comparison experiments on VQA-RAD [28], SLAKE [29] and Path-VQA [30] datasets in Table I. The proposed UniDCP demonstrates superior performance and obtains the best accuracy compared with SOTA models, including the advanced attention baselines like MFB [33], SAN [34], BAN [35], MAML [36] and MEVF [37]. Compared to advanced methods [1], [2], [4] pre-trained with the same medical datasets, our model outperforms by up to 12.3%, 8.1% and 11.4% overall accuracy on VQA-RAD respectively, indicating that UniDCP learns predominant unified medical cross-modal representations. Moreover, the improvements over the M3AE [7] which also pre-trains with multiple tasks on clinic datasets are 2.2%, 2.7% and 1.9% overall accuracy on VQA-RAD, SLAKE and Path-VQA respectively. The superior promotion demonstrates the efficacy of dynamic prompts in knowledge alignments. Besides, we observe that UniDCP can considerably exceed the VQAMix [3] which devises a special method for better adaptation. When compared with MedVInT [38] which pre-trained on the PMC-VQA dataset, our model demonstrates

TABLE II
THE COMPARISONS BETWEEN UNIDCP AND MEDICAL REPORT GENERATION METHODS ON IU X-RAY AND MIMIC-CXR DATASETS.

Methods	IU X-Ray(mean±std)					MIMIC-CXR(mean±std)				
	BLEU-1	BLEU-2	BLEU-3	BLEU-4	ROUGE-L	BLEU-1	BLEU-2	BLEU-3	BLEU-4	ROUGE-L
Show-Tell [49]	0.346	0.214	0.141	0.095	0.320	0.299	0.184	0.121	0.084	0.263
Att2in [50]	0.399	0.239	0.172	0.126	0.321	0.325	0.203	0.136	0.096	0.276
Transformer [51]	0.422	0.264	0.177	0.120	0.338	0.314	0.192	0.127	0.090	0.265
R2Gen [52]	0.470	0.304	0.219	0.165	0.371	0.353	0.218	0.145	0.103	0.277
R2GenCMN [53]	0.475	0.309	0.222	0.170	0.375	0.353	0.218	0.148	0.106	0.278
PPKED [54]	0.483	0.315	0.224	0.168	0.376	0.360	0.224	0.149	0.106	0.284
AlignTrans [55]	0.484	0.313	0.225	0.173	0.379	0.378	0.235	0.156	0.112	0.283
Clinical-BERT [8]	0.495	0.330	0.231	0.170	0.376	0.383	0.230	0.151	0.106	0.275
RAMT [5]	0.482±0.009	0.310±0.006	0.221±0.004	0.165±0.003	0.377±0.003	0.362±0.007	0.229±0.006	0.157±0.003	0.113±0.002	0.289±0.003
TriNet [56]	0.478	0.344	0.248	0.180	0.398	0.362	0.251	0.188	0.143	0.326
M2KT [57]	0.497	0.319	0.230	0.174	0.399	0.386	0.237	0.157	0.111	0.274
MPMA [6]	0.518±0.005	0.337±0.005	0.253±0.003	0.179±0.001	0.388±0.006	0.392±0.004	0.246±0.004	0.166±0.002	0.122±0.003	0.295±0.002
Ours	0.527±0.009	0.349±0.010	0.267±0.011	0.195±0.009	0.421±0.008	0.416±0.007	0.271±0.009	0.199±0.011	0.148±0.010	0.335±0.009

TABLE III

THE EXPERIMENTS ON THE MEDICAL IMAGE CLASSIFICATION TASK AND MEDICAL SEMANTIC SEGMENTATION TASK. *: RE-IMPLEMENT RESULT. -C: PRE-TRAINED ON CHEXPert DATASET. -M: PRE-TRAINED ON MIMIC-CXR DATASET. WE CONDUCTED THE MEAN ACCURACY AND STANDARD DEVIATION BY 5 RUNS UNDER 5 DIFFERENT SEEDS. †: THE 70/15/15% TRAIN/VAL/TEST SPLITTING AND SETTINGS OF SIIM DATASET.

Methods	Medical Image Classification						Medical Semantic Segmentation(Dice)					
	CheXpert			RSNA Pneumonia			SIIM			RSNA		
	1%	10%	100%	1%	10%	100%	1%	10%	100%	1%	10%	100%
ConVIRT-C [40]	85.9	86.8	87.3	77.4	80.1	81.3	25.0	43.2	59.9	55.0	67.4	67.5
GLoRIA-C [9]	86.6	87.8	88.1	86.1	88.0	88.6	35.8	46.9	63.4	59.3	67.5	67.8
ConVIRT-M [40]	87.0	88.1	88.1	88.8	91.5	92.7	-	-	-	-	-	-
MedKLIP-M [11]	-	-	-	87.3	88.0	89.4	50.2	60.8	63.9	66.2	69.4	71.9
GLoRIA-M [9]	86.5	87.5	87.8	89.7	91.2	92.1	37.4	57.1	64.0	60.3	68.7	68.3
REFERS-M [10]	87.2	88.1	88.2	89.4	91.6	92.7	-	-	-	-	-	-
M3AE*-M [7]	86.2	87.3	87.9	89.0	90.8	92.3	52.3	61.2	64.0	67.8	70.2	72.6
MRM*-M [12]	88.5±0.7	88.5±0.6	88.7±0.3	91.3±0.6	92.7±0.4	93.3±0.4	51.4±0.8	62.3±1.1	64.8±0.9	68.5±0.9	71.3±0.6	74.7±0.8
CheXzero-M [58]	-	-	88.9	-	-	-	-	-	-	-	-	-
KAD-M [59]	-	-	90.5	-	-	-	-	-	-	-	-	-
MPMA-M [6]	89.1±0.8	89.8±0.5	90.6±0.4	91.3±0.6	93.4±0.5	94.1±0.3	-	-	-	-	-	-
Ours-M	90.5±0.9	91.2±0.6	91.9±1.0	93.1±0.7	94.6±0.8	95.2±1.1	57.8±0.8	63.4±0.9	65.5±0.9	73.8±0.7	75.4±0.9	77.9±1.0
MRM†-M [12]	88.5±0.7	88.5±0.6	88.7±0.3	91.3±0.6	92.7±0.4	93.3±0.4	-	73.2±0.5	91.4±0.3	68.5±0.9	71.3±0.6	74.7±0.8
Ours†-M	90.5±0.9	91.2±0.6	91.9±1.0	93.1±0.7	94.6±0.8	95.2±1.1	-	74.5±0.7	92.4±0.6	73.8±0.7	75.4±0.9	77.9±1.0

TABLE IV

THE EXPERIMENTS ON MEDICAL IMAGE-TEXT CLASSIFICATION AND RETRIEVAL TASKS OVER THE MELINDL AND ROCO TEST SET.

Methods	MELINDA		ROCO(%)					
	Test Acc	T2I			I2T			
		R@1	R@5	R@10	R@1	R@5	R@10	
VILT [60]	-	9.75	28.95	41.40	11.90	31.90	43.20	
METER [61]	-	11.30	27.25	39.60	14.45	33.30	45.10	
CPRD+BAN [4]	75.7±0.8	15.40±0.9	35.87±0.8	43.45±1.0	17.12±1.1	38.26±0.9	54.76±1.0	
PubMedCLIP [2]	76.3±0.8	16.92±1.1	38.89±0.8	49.31±1.1	18.02±0.9	40.58±1.0	56.43±1.2	
M3AE [7]	78.5	19.05	47.75	61.35	19.10	45.60	61.20	
Ours	79.6±0.5	22.40±0.6	53.10±0.9	66.90±1.0	23.40±0.8	51.30±0.9	66.00±0.9	

superior performance, achieving improvements of over 1.1% on the VQA-RAD dataset and 1.5% on the SLAKE dataset, indicating the superior generalization.

2) *Medical Report Generation*: We adopt the IU X-Ray and MIMIC-CXR (test-set) for evaluating the similarity scores (e.g. BLUE, BOUGE-L) between the generated and labeled reports. As shown in Table II, our model is superior to the attention works Show-Tell [49], Att2in [51] and Transformer [50], and achieves 0.421 and 0.335 on the ROUGE-L of IU X-Ray and MIMIC-CXR respectively. Specifically, the improvements over the advanced works R2Gen [52], R2GenCMN [53], PPKED [54], AlignTrans [55] without pre-training are 0.030, 0.025, 0.027, 0.022 and 0.045, 0.042, 0.042, 0.036 of the BLUE-4 on two datasets respectively. Also, our model outperforms the SOTA works Clinical-BERT [8] which pre-trains

TABLE V

THE EXPERIMENTS ON MEDICAL NATURAL LANGUAGE INFERENCE(NLI) AND QUESTION ANSWERING TASK. *: RE-IMPLEMENT.

Methods	NLI	Question Answering	
	MedNLI(%)	PubMedQA(%)	BioAsq(%)
BioBERT [62]	82.63	60.24	84.14
ClinicalBERT [63]	82.70	49.08	68.50
ChestXRayBERT* [64]	83.12	49.55	69.19
T5* [65]	83.90	49.68	75.82
BlueBERT [66]	84.00	48.44	68.71
PubMedBERT [16]	84.17	55.84	87.56
BioELECTRA [67]	86.34	64.02	88.57
SciFive [68]	86.50	-	-
Ours	87.70±0.8	66.12±0.9	90.01±0.8

on the domain-specific clinic datasets, M2KT [57] which is equipped with the knowledge graph, RAMT [5], TriNet [56] and MPMA [6] by up to 0.060, 0.061, 0.046, 0.009 and 0.040 on the ROUGE-L of MIMIC-CXR dataset, respectively. A possible explanation could be that the learned visual and textual prompts benefit the cognizant of the medical images and thus further generate more comprehensive clinic reports.

3) *Medical Image Classification and Segmentation*: We compare UniDCP with advanced works through labeling 1%, 10% and 100% ratios of CheXpert and RSNA Pneumonia datasets of classification and SIIM, RSNA of segmentation task in Table III. UniDCP outperforms SOTA works [7],

TABLE VI

ABLATION STUDY ON THE SLAKE, MIMIC-CXR(TEST-SET) AND THE RSNA DATASETS. ‘‘PROMPT’’ REPRESENTS THE DYNAMIC VISUAL/TEXTUAL PROMPTS OPTIMIZING STRATEGY. ‘‘MULTI-TASK’’ IS THE UNIFIED MODEL JOINTLY OPTIMIZED WITH MULTIPLE PRE-TRAINING TASKS.

Prompt	Multi-task	SLAKE(%)			MIMIC-CXR				RSNA Pneumonia(%)			
		Open	Closed	All	BLEU-1	BLEU-2	BLEU-3	BLEU-4	ROUGE-L	1%	10%	100%
×	×	79.8±1.2	83.9±1.0	81.6±1.2	0.314±0.006	0.192±0.008	0.127±0.005	0.090±0.006	0.265±0.004	87.5±1.1	88.2±0.9	89.5±1.2
✓	×	83.7±1.4	88.5±1.3	85.5±1.1	0.381±0.008	0.286±0.007	0.184±0.004	0.133±0.007	0.319±0.005	91.3±1.0	91.8±1.0	93.7±1.1
×	✓	83.1±1.1	87.5±1.2	84.6±1.2	0.379±0.006	0.247±0.007	0.174±0.005	0.120±0.005	0.307±0.007	91.7±1.2	92.4±1.1	93.9±1.3
✓	✓	84.0±1.2	88.9±0.9	85.9±1.1	0.416±0.005	0.271±0.006	0.199±0.006	0.148±0.007	0.335±0.005	93.1±1.2	94.6±1.0	95.2±1.1

TABLE VII

ABLATION STUDY OF VARIOUS PROMPT METHODS WHICH CONTAINS THE STATIC TEXTUAL PROMPT, VISUAL PROMPT AND THE PROPOSED DYNAMIC CROSS-MODAL PROMPTS ON THE SLAKE, VQA-RAD, MELINDA DATASETS.

Prompt strategy			SLAKE(%)			VQA-RAD(%)			MELINDA(%)	
Textual Prompt	Visual Prompt	Dynamic Prompts	Open	Closed	Overall	Open	Closed	Overall	Accuracy	
×	×	×	81.0±1.3	85.2±1.2	82.5±1.3	66.4±1.2	82.5±1.1	77.1±1.2	77.8±1.2	
✓	×	×	81.3±1.2	85.4±1.3	82.9±1.2	66.6±1.1	82.8±1.2	77.4±1.2	78.0±1.4	
×	✓	×	81.5±1.1	85.5±1.0	83.0±1.1	66.7±1.1	83.0±1.3	77.5±1.4	78.2±1.4	
✓	✓	×	81.8±1.4	86.2±1.3	83.5±1.4	66.9±1.3	83.0±1.4	77.6±1.3	78.1±1.3	
×	×	✓	84.0±1.0	88.9±1.1	85.9±1.1	68.5±1.4	84.4±1.1	79.2±1.3	79.6±1.3	

TABLE VIII

ABLATION STUDY OF MULTIPLE PRE-TRAINING TASKS ACROSS THE VQA-RAD, IU X-RAY AND CHEXPART DATASETS.

Pre-training Tasks	VQA-RAD(%)			IU X-Ray				CheXpert(%)				
	Open	Closed	All	BLEU-1	BLEU-2	BLEU-3	BLEU-4	METEOR	ROUGE_L	1%	10%	100%
MLM	66.2±1.3	83.9±1.2	77.8±1.3	0.493±0.008	0.333±0.006	0.248±0.005	0.174±0.007	0.232±0.006	0.410±0.005	90.1±1.3	90.3±1.0	90.2±1.1
MLM+ITM	67.1±1.1	84.0±1.0	78.3±1.2	0.509±0.006	0.335±0.005	0.252±0.004	0.182±0.005	0.239±0.006	0.421±0.006	90.2±1.1	90.3±1.1	91.4±1.2
MLM+ITC	67.8±1.2	84.2±1.0	78.7±1.2	0.514±0.006	0.338±0.006	0.256±0.005	0.188±0.005	0.243±0.004	0.422±0.004	90.3±1.0	90.5±1.1	91.4±1.1
MLM+ITC+ITM	68.1±1.0	84.4±1.1	79.0±1.1	0.528±0.007	0.343±0.004	0.267±0.004	0.196±0.006	0.251±0.005	0.423±0.004	90.5±1.2	90.8±1.3	91.7±1.0

TABLE IX

ABLATION STUDY OF PROMPTS. +P: PRE-TRAIN WITH PROMPT. VP-N: SELECT N VISUAL PROMPTS, TP-N: SELECT N TEXTUAL PROMPTS.

Settings	MLM	+P	ITM	ITM+P	VP-16	-49	-64	TP-16	-32	-48
SLAKE(Overall)	83.8	85.6	83.3	85.3	85.8	86.0	85.6	85.9	86.1	85.7
CheXpert(100%)	88.2	90.3	88.4	90.1	91.2	91.6	91.4	91.0	91.4	91.3
add-Memory(G)	-	2.3	-	1.4	0.9	1.3	2.2	0.4	0.5	0.7
add-Param(M)	-	0.88	-	0.93	0.19	0.59	0.77	0.14	0.29	0.43

TABLE X

ABLATION STUDY OF THE SIZE OF PROMPT SPACE M, J.

M	512			1024			2048		
	512	1024	2048	512	1024	2048	512	1024	2048
SLAKE(Overall)	84.7	84.9	84.8	85.0	85.6	84.9	84.8	85.0	84.9
CheXpert(100%)	91.0	91.2	91.1	91.3	91.7	91.2	91.0	91.1	91.0
MedNLI	87.4	87.6	87.5	87.4	87.7	87.5	87.3	87.4	87.4

[9]–[12], [40], [58], [59] under different label ratios over 4 datasets. Specifically, when labeling a few datasets like 1% and 10%, UniDCP obtains 1.4%, 1.4% and 1.8%, 1.2% improvements compared with the SOTA work MPMA-M [6] on the CheXpert and RSNA datasets, and 6.4%, 1.1% and 5.3%, 4.1% compared with the SOTA work MRM [12] on SIIM and RSNA respectively. This demonstrates the superior generalization of UniDCP with few labeled datasets. Besides, for 100% ratio, UniDCP has improved by 1.3% and 1.1% on both datasets compared with the SOTA work MPMA [6]. In addition, under various data partitioning schemes of SIIM [42] (70%/15%/15% for MRM† [12] and 70%/30%/30% for MRM [12] in Table III), our model consistently demonstrates superior performance, illustrating that the unified model benefits from shareable clinic knowledge.

TABLE XI

ABLATION STUDY OF PRE-TRAINING DATASETS. -M: PRE-TRAINED ON THE MIMIC-CXR, -M,R: PRE-TRAINED ON MIMIC-CXR AND ROCO.

Methods	VQA-RAD			CheXpert			MELINDA
	Open	Closed	Overall	1%	10%	100%	Accuracy
M3AE [7]	67.2	83.5	77.0	86.2	87.3	87.9	78.5
Ours-M	68.0±1.3	84.1±1.2	78.8±1.3	90.0±0.9	90.8±0.7	91.2±0.8	79.2±0.6
Ours-M, R	68.5±1.2	84.4±1.1	79.2±1.3	90.5±0.6	91.2±0.8	91.9±0.8	79.6±0.7

TABLE XII

ABLATION STUDY OF LINGUAL BIOMEDICAL PRE-TRAINING DATASETS. -O: PRE-TRAINED ON THE ORIGINAL MED-VLP DATASETS. -P: PRE-TRAINED ON THE BIOMEDICAL DOMAIN-SPECIFIC CORPORA.

Methods	Lingual Pre-train Data	MedNLI	PubMedQA	BioAsq
BioELECTRA [67]	PMC, PubMed	86.34	64.02	88.57
SciFive [68]	PMC, PubMed	86.50	-	-
Ours-O	-	87.70±1.3	66.12±1.2	90.01±1.3
Ours-P	PMC, PubMed	88.25±1.2	66.98±1.1	90.56±1.2

4) *Natural Language Inference and Question Answering:*

As shown in Table V, we conduct comparisons on the medical natural language inference task over the MedNLI and question-answering task on PubMedQA and BioAsq. It should be noted that UniDCP achieves SOTA results compared with advanced BERT-based text-to-text methods like BioBERT [62], ClinicalBERT [63], ChestXRayBERT [64], T5 [65], BlueBERT [66], PubMedBERT [16], BioELECTRA [67] and yields 87.70%, 66.12% and 90.01% accuracy on triple datasets. Explicitly, UniDCP considerably surpasses the SciFive [68] which is a domain-specific model pre-trained on large biomedical corpora by 1.20% on MedNLI. These demonstrate that UniDCP is highly versatile to medical text tasks with learned clinic knowledge.

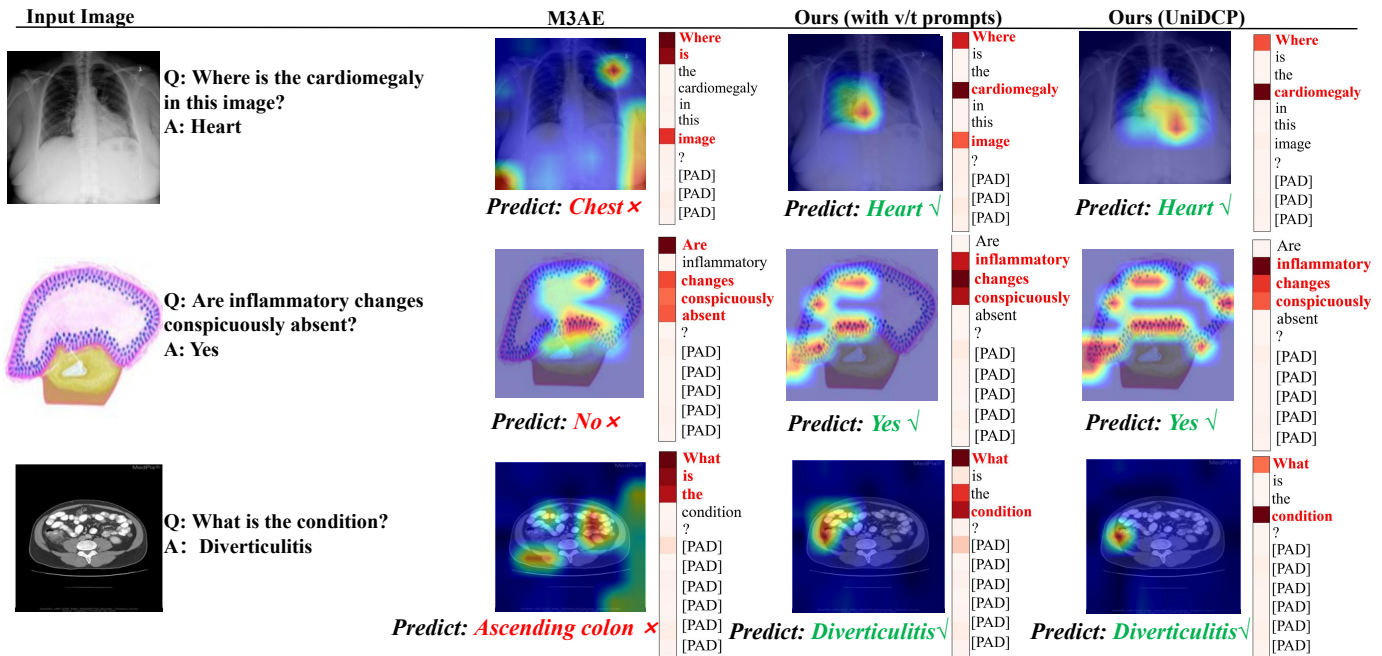


Fig. 3. The qualitative analysis is conducted on the Med-VQA tasks. First column: input image and question-answer pair. The second column to the last contains the cross-modal attention maps of the M3AE [7], the baseline equipped with the dynamic vision-language prompts and the proposed UniDCP model.




Image	Ground Truth	MPMA	Ours
	No there is an dextroscoliosis of the thoracic spine. The cardiomeastinal silhouette and pulmonary vasculature are within normal limits. There is no pneumothorax or pleural effusion. There are no focal areas of consolidation.	The presence of dextroscoliosis is noted in the thoracic spine . The pulmonary vasculature exhibit normal characteristics. No indications of pneumothorax are identified, and there is an absence of focal areas of consolidation .	Dextroscoliosis is observed in the thoracic spine . The cardiomeastinal silhouette and pulmonary vasculature are within the normal limits . Absence of pneumothorax or pleural effusion is noted, and there are no focal regions of consolidation .
	The cardio mediastinal silhouette is within normal limits for size and contour. The lungs are normally inflated without evidence of focal airspace disease, pleural effusion, or pneumothorax. Osseous structures are within normal limits for patient age..	The cardio mediastinal silhouette exhibits normal dimensions and contours . The lungs are adequately inflated , showing no indications of focal airspace abnormalities, pleural effusion .	The cardio mediastinal silhouette outlines appear normal in size and shape . The lungs exhibit normal inflation without signs of localized airspace disease, pleural effusion, or pneumothorax . Osseous structures are within normal limits for the patient's age.
	Low lung volumes are present. The heart size and pulmonary vascularity appear within normal limits. Lungs are free of focal airspace disease. No pleural effusion or pneumothorax is seen. Surgical clips are present in the abdomen.	Reduced lung volumes are noted. The cardiac dimensions and pulmonary vascular patterns appear unremarkable. The lungs exhibit no discernible focal airspace pathology. There is an absence of pleural effusion or pneumothorax .	There are low lung volumes observed. The heart size and the pulmonary vasculature seems to be within the normal range. The lungs exhibit an absence of focal airspace disease . No signs of pleural effusion or pneumothorax are evident. Surgical clips are detected in the abdominal region.

Fig. 4. The additional qualitative analysis is conducted on the medical report generation tasks across IU X-ray dataset. First column: Input medical image. Second column: the ground truth reports. Third column: the generated report of the SOTA model MPMA [6]. The last column: the generated report of ours. The indication in Green: the correctly predicted MeSH terms.

5) *Medical Image-text Classification and Retrieval*: We fine-tune UniDCP on the medical image-text classification and retrieval tasks. As shown in Table IV, UniDCP has significant improvement compared with the advanced works [2], [4]. In particular, although the M3AE enhances the visual-textual representations and yields 78.5% accuracy, UniDCP improves the accuracy by 1.1%. This illustrates that UniDCP could grasp unified representations for precise classification. Besides, our model is superior to the advanced cross-modal pre-training works ViLT [60], METER [61] and considerably surpasses the M3AE by 3.35%, 5.35% and 5.55% with Recall@1, 5, 10 of text-to-image retrieval. This demonstrates that UniDCP has excellent plasticity of medical vision-textual knowledge.

B. Ablation Study

1) *Ablation Study of the Proposed Methods*: As shown in Table VI, we conduct the ablation study to verify the effec-

tiveness of the proposed methods, including the unified model optimized with multiple pre-training tasks and the dynamic cross-modal prompts optimizing strategy. For row 1 in Table VI, we take the dual-encoder with uni-modal inputs and pre-train with a single MLM task as the baseline. For row 2, the baseline equipped with dynamic prompts optimizing strategy obtains 3.9% overall accuracy on SLAKE, 0.043 and 0.064 of BLEU-4 and ROUGE-L on MIMIC-CXR, 3.8%, 3.6% and 4.2% of the three different labeled ratios on RSNA Pneumonia. This demonstrates that the dynamic cross-modal prompts unify the vision-language inputs and share the clinic knowledge for better understanding, bringing obvious improvements in medical uni-modal and cross-modal tasks.

For row 3 in Table VI, the baseline is adapted to the unified model pre-trained with MLM, ITM and ITC tasks, obtaining 3.0% improvements on SLAKE, 0.030 and 0.042 of BLEU-4 and ROUGE-L on MIMIC-CXR, 4.2%, 4.2% and 4.4%

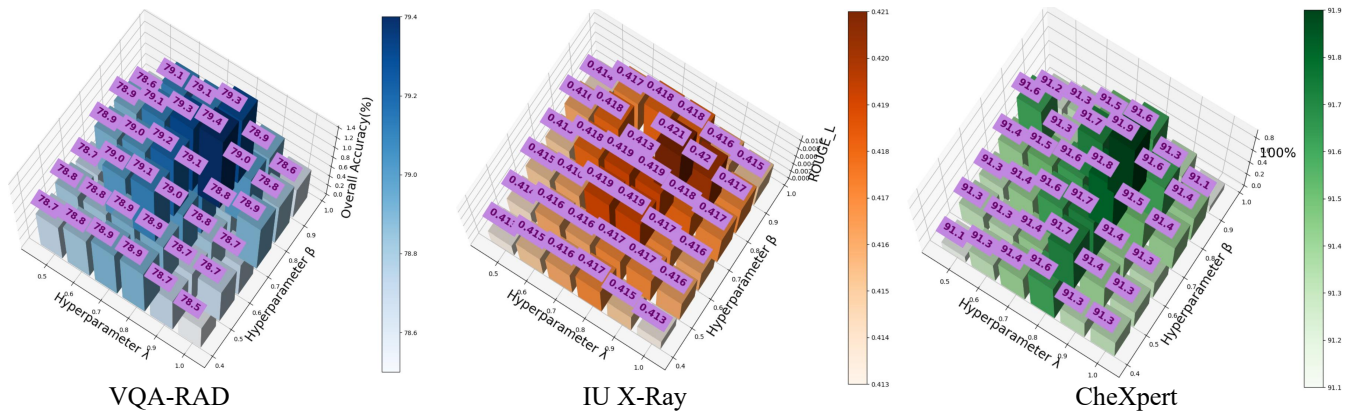


Fig. 5. The influence experiments of the loss balancing hyperparameters λ and β on the VQA-RAD, IU X-Ray and CheXpert datasets.

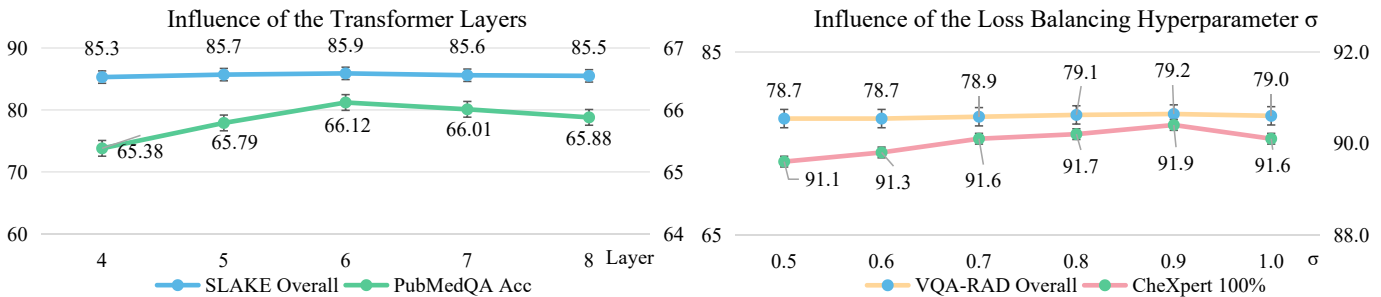


Fig. 6. Influence of the transformer layers in the unified model and the influence experiments of the loss balancing hyperparameters σ .

on RSNA Pneumonia. It illustrates the unified model with multiple pre-training tasks benefits downstream tasks with shareable knowledge. Moreover, we also take a further step to demonstrate the effectiveness of each pre-training task in Table XI and figure out that the ITC task observes the most significant improvements for the alignment.

Accordingly, the unified baseline jointly equipped with the dynamic prompts optimizing strategy and multiple pre-training tasks observes the best result which reaches 85.9% overall accuracy on SLAKE, 0.335 of ROUGE-L on MIMIC-CXR, 93.1%, 94.6% and 95.2% on RSNA Pneumonia, suggesting that our proposed model grasps efficient clinic knowledge and the unified cross-modal representations and then adapt to multiple fine-tuning tasks flexibly.

2) *Ablation Study of Dynamic Prompts Strategy*: We offer an ablation study of distinct prompt methodologies, encompassing static visual/textual prompts and the novel dynamic prompt strategy, as depicted in Table VII. The experiments unveil that static visual and textual prompts yield minimal enhancements across multiple medical fine-tuning tasks. Conversely, the introduced dynamic cross-modal prompts exhibit substantial superiority across both tasks. This demonstrates the advantage of dynamic prompts in integrating shared medical information across multiple downstream tasks.

3) *Ablation Study of Pre-training Tasks*: We conduct the ablation study of multiple pre-training tasks within a unified model in Table VIII. The experiments on the VQA-RAD, IU X-Ray and CheXpert datasets illustrate the effectiveness of each pre-training task and the ITC task observes the most significant improvement.

4) *Ablation Study of Pre-training Datasets*: Table XI illustrates the ablation study of Med-VLP pre-training datasets. It reveals that while pre-training UniDCP with a single pre-training dataset may lead to a decrease in performance, our framework still offers advantages compared to state-of-the-art method M3AE [7] across the SLAKE, CheXpert, and MELINDA datasets. This is attributed to the incorporation of the unified structure jointly with the dynamic prompt optimizing strategy to incorporate clinic knowledge into multiple medical uni-modal and cross-modal tasks.

5) *Lingual Biomedical Pre-training Datasets*: As shown in Table XII, the ablation study of the lingual biomedical pre-training datasets is adopted in the medical natural language inference task and the medical question answering task. From the ablation study, it is evident that even without specialized pre-training on medical text datasets like PubMed abstracts (PubMed) [45] and PubMed Central full-text articles (PMC) [38], our model can achieve remarkable performance compared with the SOTA methods like BioELECTRA [67] and SciFive [68]. Furthermore, when we utilize the same Lingual biomedical datasets PMC and PubMed for pre-training, more pronounced improvements are attainable across the MedNLI, PubMedQA and BioAqa datasets.

6) *Addition Memory and Parameter Cost*: We conducted the ablation study to examine how the inclusion of different numbers of learnable visual/textual prompts affects additional memory and parameter costs, as detailed in Table IX. Besides, Table X illustrates the ablation study of M , J in Eq. 3. These reveal that the dynamic prompts achieve minimal memory cost, and more importantly, the selection of effective prompts

is more useful than the construction of more of them.

C. Qualitative Analysis

As shown in Fig. 3, we conduct a detailed qualitative analysis through the Grad-CAM to figure out how a unified model with dynamic prompts helps medical vision-language prediction. Besides, we also demonstrate the model's superior ability to generate accurate and semantically meaningful medical reports in Fig. 4.

Specifically, for the abdominal CT selected from VQA-RAD [28], the proposed UniDCP can precisely indicate the keywords "What, condition" with the precise visual object rather than the meaningless words "is the" and the irrelevant intestinal parts (e.g. the black background) the M3AE [7] focuses on. Moreover, we can witness the prominent gains in the unification of the vision/text features from the second column to the fourth, the highlighted vision objects and keywords are closely semantically related and conduct the correct prediction in a unified manner. The comparison demonstrates that UniDCP exhibits exceptional unification capabilities and effectively identifies precise clinical vision and textual features to facilitate unified cross-modal representations.

Besides, while the baseline equipped with dynamic vision-language prompts suffices to highlight the relatively coarse parts of black diverticulitis and the keywords with lightweight, UniDCP distinctly centers on a more specific visual object of diverticulitis and keywords with more distinct weights for indication. It demonstrates the effectiveness of the dynamic prompts for learning the shareable clinic information and further illustrates importance of the unified model for more precise cross-modal representations.

D. Influence Analysis

1) *Influence of Layers Within Unified Model:* As shown in Fig. 6, we also conduct the influence experiment on the transformer layer of the unified model across SLAKE [29], RSNA [43] and PubMedQA [45]. It can be witnessed that the unified model composed of 6 transformer layers obtains the best results on the medical uni-modal and cross-modal tasks.

2) *Influence of Hyperparameters:* In this section, we conduct the influence experiment on the VQA-RAD, IU X-Ray, and CheXpert datasets of different hyperparameters illustrated in Fig. 5 and Fig. 6. We assign the hyperparameters σ , λ and β from 0.5 to 1.0 with step 0.1 and attach the best result when σ is set to 0.9, λ is 0.8, and β is 0.9. The stable experiment results illustrate the generalization and robustness of our proposed method.

VI. CONCLUSION

In this paper, we construct a unified and plastic Med-VLP model for multiple medical vision-language tasks. Our approach first dynamically selects visual/textual prompts within the shareable prompts space for harmonizing diverse inputs. The joint optimization of the dynamic prompts and the unified model alongside multiple pre-training tasks, facilitates the alignment of cross-modal representations while adapting the

wealth of shareable information to multiple fine-tuning tasks. The proposed framework exhibits superior performance on 8 medical vision-language tasks over 14 corresponding datasets, illustrating the outstanding scalability of UniDCP. In future exploration, we plan to construct a novel generative model that can handle more combinations of medical modalities. Codes will be released.

REFERENCES

- [1] Y. Khare, V. Bagal, M. Mathew, A. Devi, U. D. Priyakumar, and C. Jawahar, "Mmbert: multimodal bert pretraining for improved medical vqa," in *2021 IEEE 18th International Symposium on Biomedical Imaging (ISBI)*. IEEE, 2021, pp. 1033–1036.
- [2] S. Eslami, G. de Melo, and C. Meinel, "Does clip benefit visual question answering in the medical domain as much as it does in the general domain?" *arXiv preprint arXiv:2112.13906*, 2021.
- [3] H. Gong, G. Chen, M. Mao, Z. Li, and G. Li, "Vqamix: Conditional triplet mixup for medical visual question answering," *IEEE TMI*, vol. 41, no. 11, pp. 3332–3343, 2022.
- [4] B. Liu, L.-M. Zhan, and X.-M. Wu, "Contrastive pre-training and representation distillation for medical visual question answering based on radiology images," in *MICCAI*. Springer, 2021, pp. 210–220.
- [5] K. Zhang, H. Jiang, J. Zhang, Q. Huang, J. Fan, J. Yu, and W. Han, "Semi-supervised medical report generation via graph-guided hybrid feature consistency," *IEEE Transactions on Multimedia*, 2023.
- [6] K. Zhang, Y. Yang, J. Yu, H. Jiang, J. Fan, Q. Huang, and W. Han, "Multi-task paired masking with alignment modeling for medical vision-language pre-training," *IEEE Transactions on Multimedia*, 2023.
- [7] Z. Chen, Y. Du, J. Hu, Y. Liu, G. Li, X. Wan, and T.-H. Chang, "Multi-modal masked autoencoders for medical vision-and-language pre-training," in *International Conference on Medical Image Computing and Computer-Assisted Intervention*. Springer, 2022, pp. 679–689.
- [8] B. Yan and M. Pei, "Clinical-bert: Vision-language pre-training for radiograph diagnosis and reports generation," in *Proceedings of the AAAI Conference on Artificial Intelligence*, vol. 36, no. 3, 2022, pp. 2982–2990.
- [9] S.-C. Huang, L. Shen, M. P. Lungren, and S. Yeung, "Gloria: A multimodal global-local representation learning framework for label-efficient medical image recognition," in *ICCV*, 2021, pp. 3942–3951.
- [10] H.-Y. Zhou, X. Chen, Y. Zhang, R. Luo, L. Wang, and Y. Yu, "Generalized radiograph representation learning via cross-supervision between images and free-text radiology reports," *Nature Machine Intelligence*, vol. 4, no. 1, pp. 32–40, 2022.
- [11] C. Wu, X. Zhang, Y. Zhang, Y. Wang, and W. Xie, "Medklip: Medical knowledge enhanced language-image pre-training," *medRxiv*, pp. 2023–01, 2023.
- [12] H.-Y. Zhou, C. Lian, L. Wang, and Y. Yu, "Advancing radiograph representation learning with masked record modeling," *arXiv preprint arXiv:2301.13155*, 2023.
- [13] K. Zhou, J. Yang, C. C. Loy, and Z. Liu, "Conditional prompt learning for vision-language models," in *CVPR*, 2022, pp. 16 816–16 825.
- [14] Zhou, Kaiyang and Yang, Jingkang and Loy, Chen Change and Liu, Ziwei, "Learning to prompt for vision-language models," *International Journal of Computer Vision*, vol. 130, no. 9, pp. 2337–2348, 2022.
- [15] Y. Zang, W. Li, K. Zhou, C. Huang, and C. C. Loy, "Unified vision and language prompt learning," *arXiv preprint arXiv:2210.07225*, 2022.
- [16] P. Gao, S. Geng, R. Zhang, T. Ma, R. Fang, Y. Zhang, H. Li, and Y. Qiao, "Clip-adapter: Better vision-language models with feature adapters," *arXiv preprint arXiv:2110.04544*, 2021.
- [17] J. Wen, F. Qin, J. Du, M. Fang, X. Wei, C. P. Chen, and P. Li, "Msfusion: Medical semantic guided two-branch network for multimodal brain image fusion," *IEEE Transactions on Multimedia*, 2023.
- [18] Z. Zhong, D. Friedman, and D. Chen, "Factual probing is [mask]: Learning vs. learning to recall," *arXiv preprint arXiv:2104.05240*, 2021.
- [19] X. L. Li and P. Liang, "Prefix-tuning: Optimizing continuous prompts for generation," *arXiv preprint arXiv:2101.00190*, 2021.
- [20] B. Lester, R. Al-Rfou, and N. Constant, "The power of scale for parameter-efficient prompt tuning," *arXiv preprint arXiv:2104.08691*, 2021.
- [21] M. Jia, L. Tang, B.-C. Chen, C. Cardie, S. Belongie, B. Hariharan, and S.-N. Lim, "Visual prompt tuning," in *European Conference on Computer Vision*. Springer, 2022, pp. 709–727.

- [22] Y. Xing, Q. Wu, D. Cheng, S. Zhang, G. Liang, P. Wang, and Y. Zhang, "Dual modality prompt tuning for vision-language pre-trained model," *IEEE Transactions on Multimedia*, 2023.
- [23] Z. Chen, S. Diao, B. Wang, G. Li, and X. Wan, "Towards unifying medical vision-and-language pre-training via soft prompts," *arXiv preprint arXiv:2302.08958*, 2023.
- [24] A. Van Den Oord, O. Vinyals *et al.*, "Neural discrete representation learning," *Advances in neural information processing systems*, vol. 30, 2017.
- [25] L. H. Li, M. Yatskar, D. Yin, C.-J. Hsieh, and K.-W. Chang, "Visualbert: A simple and performant baseline for vision and language," *arXiv preprint arXiv:1908.03557*, 2019.
- [26] O. Pelka, S. Koitka, J. Rückert, F. Nensa, and C. M. Friedrich, "Radiology objects in context (roco): A multimodal image dataset," in *Intravascular Imaging and Computer Assisted Sienting and Large-Scale Annotation of Biomedical Data and Expert Label Synthesis*, 2018, pp. 180–189.
- [27] A. E. Johnson, T. J. Pollard, N. R. Greenbaum, M. P. Lungren, C.-y. Deng, Y. Peng, Z. Lu, R. G. Mark, S. J. Berkowitz, and S. Horng, "Mimic-cxr-jpg, a large publicly available database of labeled chest radiographs," *arXiv preprint arXiv:1901.07042*, 2019.
- [28] J. J. Lau, S. Gayen, A. Ben Abacha, and D. Demner-Fushman, "A dataset of clinically generated visual questions and answers about radiology images," *Scientific data*, vol. 5, p. 180251, 2018.
- [29] B. Liu, L.-M. Zhan, L. Xu, L. Ma, Y. Yang, and X.-M. Wu, "Slake: A semantically-labeled knowledge-enhanced dataset for medical visual question answering," in *2021 IEEE 18th International Symposium on Biomedical Imaging (ISBI)*, 2021, pp. 1650–1654.
- [30] X. He, "Towards visual question answering on pathology images," in *Proceedings of the 59th annual meeting of the association for computational linguistics and the 11th international joint conference on natural language processing*, vol. 2, 2021.
- [31] D. Demner-Fushman, M. D. Kohli, M. B. Rosenman, S. E. Shooshan, L. Rodriguez, S. Antani, G. R. Thoma, and C. J. McDonald, "Preparing a collection of radiology examinations for distribution and retrieval," *Journal of the American Medical Informatics Association*, vol. 23, no. 2, pp. 304–310, 2016.
- [32] T.-L. Wu, S. Singh, S. Paul, G. Burns, and N. Peng, "Melinda: A multimodal dataset for biomedical experiment method classification," in *Proceedings of the AAAI Conference on Artificial Intelligence*, vol. 35, no. 16, 2021, pp. 14 076–14 084.
- [33] Z. Yu, J. Yu, J. Fan, and D. Tao, "Multi-modal factorized bilinear pooling with co-attention learning for visual question answering," in *ICCV*, 2017, pp. 1821–1830.
- [34] Z. Yang, X. He, J. Gao, L. Deng, and A. Smola, "Stacked attention networks for image question answering," in *CVPR*, 2016, pp. 21–29.
- [35] J.-H. Kim, J. Jun, and B.-T. Zhang, "Bilinear attention networks," *Advances in neural information processing systems*, vol. 31, 2018.
- [36] C. Finn, P. Abbeel, and S. Levine, "Model-agnostic meta-learning for fast adaptation of deep networks," in *International conference on machine learning*. PMLR, 2017, pp. 1126–1135.
- [37] B. D. Nguyen, T.-T. Do, B. X. Nguyen, T. Do, E. Tjiputra, and Q. D. Tran, "Overcoming data limitation in medical visual question answering," in *MICCAI*. Springer, 2019, pp. 522–530.
- [38] X. Zhang, C. Wu, Z. Zhao, W. Lin, Y. Zhang, Y. Wang, and W. Xie, "Pmc-vqa: Visual instruction tuning for medical visual question answering," *arXiv preprint arXiv:2305.10415*, 2023.
- [39] J. Irvin, P. Rajpurkar, M. Ko, Y. Yu, S. Ciurea-Ilcus, C. Chute, H. Marklund, B. Haghighi, R. Ball, K. Shpanskaya *et al.*, "Chexpert: A large chest radiograph dataset with uncertainty labels and expert comparison," in *Proceedings of the AAAI conference on artificial intelligence*, vol. 33, no. 01, 2019, pp. 590–597.
- [40] Y. Zhang, H. Jiang, Y. Miura, C. D. Manning, and C. P. Langlotz, "Contrastive learning of medical visual representations from paired images and text," in *Machine Learning for Healthcare Conference*. PMLR, 2022, pp. 2–25.
- [41] G. Shih, C. C. Wu, S. S. Halabi, M. D. Kohli, L. M. Prevedello, T. S. Cook, A. Sharma, J. K. Amorosa, V. Arteaga, M. Galperin-Aizenberg *et al.*, "Augmenting the national institutes of health chest radiograph dataset with expert annotations of possible pneumonia," *Radiology: Artificial Intelligence*, vol. 1, no. 1, p. e180041, 2019.
- [42] A. Anuar, "SIIM-ACR Pneumothorax Segmentation," 2019.
- [43] G. Shih, C. C. Wu, S. S. Halabi, M. D. Kohli, L. M. Prevedello, T. S. Cook, A. Sharma, J. K. Amorosa, V. Arteaga, M. Galperin-Aizenberg *et al.*, "Augmenting the national institutes of health chest radiograph dataset with expert annotations of possible pneumonia," *Radiology: Artificial Intelligence*, vol. 1, no. 1, p. e180041, 2019.
- [44] A. Romanov and C. Shivade, "Lessons from natural language inference in the clinical domain," *arXiv preprint arXiv:1808.06752*, 2018.
- [45] Q. Jin, B. Dhingra, Z. Liu, W. W. Cohen, and X. Lu, "Pubmedqa: A dataset for biomedical research question answering," *arXiv preprint arXiv:1909.06146*, 2019.
- [46] A. Nentidis, K. Bougiatiotis, A. Krithara, and G. Paliouras, "Results of the seventh edition of the bioasq challenge," in *Machine Learning and Knowledge Discovery in Databases: International Workshops of ECML PKDD 2019, Würzburg, Germany, September 16–20, 2019, Proceedings, Part II*. Springer, 2020, pp. 553–568.
- [47] A. Radford, J. W. Kim, C. Hallacy, A. Ramesh, G. Goh, S. Agarwal, G. Sastry, A. Askell, P. Mishkin, J. Clark *et al.*, "Learning transferable visual models from natural language supervision," in *International conference on machine learning*. PMLR, 2021, pp. 8748–8763.
- [48] Y. Liu, M. Ott, N. Goyal, J. Du, M. Joshi, D. Chen, O. Levy, M. Lewis, L. Zettlemoyer, and V. Stoyanov, "Roberta: A robustly optimized bert pretraining approach," *arXiv preprint arXiv:1907.11692*, 2019.
- [49] O. Vinyals, A. Toshev, S. Bengio, and D. Erhan, "Show and tell: A neural image caption generator," in *CVPR*, 2015, pp. 3156–3164.
- [50] S. J. Rennie, E. Marcheret, Y. Mroueh, J. Ross, and V. Goel, "Self-critical sequence training for image captioning," in *CVPR*, 2017, pp. 7008–7024.
- [51] A. Vaswani, N. Shazeer, N. Parmar, J. Uszkoreit, L. Jones, A. N. Gomez, Ł. Kaiser, and I. Polosukhin, "Attention is all you need," *Advances in neural information processing systems*, vol. 30, 2017.
- [52] Z. Chen, Y. Song, T.-H. Chang, and X. Wan, "Generating radiology reports via memory-driven transformer," *arXiv preprint arXiv:2010.16056*, 2020.
- [53] Z. Chen, Y. Shen, Y. Song, and X. Wan, "Cross-modal memory networks for radiology report generation," *arXiv preprint arXiv:2204.13258*, 2022.
- [54] F. Liu, X. Wu, S. Ge, W. Fan, and Y. Zou, "Exploring and distilling posterior and prior knowledge for radiology report generation," in *CVPR*, 2021, pp. 13 753–13 762.
- [55] D. You, F. Liu, S. Ge, X. Xie, J. Zhang, and X. Wu, "Aligntransformer: Hierarchical alignment of visual regions and disease tags for medical report generation," in *MICCAI*, 2021.
- [56] Y. Yang, J. Yu, J. Zhang, W. Han, H. Jiang, and Q. Huang, "Joint embedding of deep visual and semantic features for medical image report generation," *IEEE Transactions on Multimedia*, 2021.
- [57] S. Yang, X. Wu, S. Ge, Z. Zheng, S. K. Zhou, and L. Xiao, "Radiology report generation with a learned knowledge base and multi-modal alignment," *Medical Image Analysis*, vol. 86, p. 102798, 2023.
- [58] E. Tiu, E. Talius, P. Patel, C. P. Langlotz, A. Y. Ng, and P. Rajpurkar, "Expert-level detection of pathologies from unannotated chest x-ray images via self-supervised learning," *Nature Biomedical Engineering*, vol. 6, no. 12, pp. 1399–1406, 2022.
- [59] X. Zhang, C. Wu, Y. Zhang, W. Xie, and Y. Wang, "Knowledge-enhanced visual-language pre-training on chest radiology images," *Nature Communications*, vol. 14, no. 1, p. 4542, 2023.
- [60] W. Kim, B. Son, and I. Kim, "Vilt: Vision-and-language transformer without convolution or region supervision," in *International Conference on Machine Learning*. PMLR, 2021, pp. 5583–5594.
- [61] Z.-Y. Dou, Y. Xu, Z. Gan, J. Wang, S. Wang, L. Wang, C. Zhu, P. Zhang, L. Yuan, N. Peng *et al.*, "An empirical study of training end-to-end vision-and-language transformers," in *CVPR*, 2022, pp. 18 166–18 176.
- [62] J. Lee, W. Yoon, S. Kim, D. Kim, S. Kim, C. H. So, and J. Kang, "Biobert: a pre-trained biomedical language representation model for biomedical text mining," *Bioinformatics*, vol. 36, no. 4, pp. 1234–1240, 2020.
- [63] K. Huang, J. Altaaar, and R. Ranganath, "Clinicalbert: Modeling clinical notes and predicting hospital readmission," *arXiv preprint arXiv:1904.05342*, 2019.
- [64] X. Cai, S. Liu, J. Han, L. Yang, Z. Liu, and T. Liu, "Chestxraybert: A pretrained language model for chest radiology report summarization," *IEEE Transactions on Multimedia*, 2021.
- [65] M. Kale and A. Rastogi, "Text-to-text pre-training for data-to-text tasks," *arXiv preprint arXiv:2005.10433*, 2020.
- [66] Y. Peng, Q. Chen, and Z. Lu, "An empirical study of multi-task learning on bert for biomedical text mining," *arXiv preprint arXiv:2005.02799*, 2020.
- [67] K. raj Kanakarajan, K. Kundumani, B. Kundumani, and M. Sankarababu, "Bioelectra: pretrained biomedical text encoder using discriminators," in *Proceedings of the 20th Workshop on Biomedical Language Processing*, 2021, pp. 143–154.
- [68] L. N. Phan, J. T. Anibal, H. Tran, S. Chanana, E. Bahadroglu, A. Peltekian, and G. Altan-Bonnet, "Scifive: a text-to-text transformer model for biomedical literature," *arXiv preprint arXiv:2106.03598*, 2021.